Tunable Channelized Bandstop Passive Filter Using Reconfigurable Phase Shifter

R. Lababidi[1], M. Al Shami[1], M. Le Roy[1], D. Le Jeune[1], K. Khoder[2] and A. Pérennec[1]

[1]Lab-STICC (UMR CNRS 6285), ENSTA Bretagne, Université de Brest (UBO), Brest, France.
[*]raafat.lababidi@ensta-bretagne.fr
[2] Department of Innovation and Technology, Azm Institute, Rafic Hariri Avenue, Tripoli 1300, Lebanon

A novel tunable channelized two-branches passive bandstop filter using a reconfigurable parallel-coupled-line-based Phase Shifter (PS) is presented. The filter topology uses the signal destructive principle and aims to protect the receiver against an unwanted interference signal received by the antenna. The global filter topology contains two branches, each of which has a different function. The bandpass tunable branch selects the frequency to be rejected while the reconfigurable PS plays the signal invertor role. The simultaneous tunability of both bandpass and PS branches is ensured by using identical varactor diodes and features 550-700 MHz tuning range. In addition of having a constant and relatively high rejection level over all the tuning range and low insertion loss in the passband area, the filter guaranties ultra-low power consumption. Moreover, synthesis equations are proposed and used to illustrate the operating principle, and finally validated by comparing simulations results to measurements.

1. Introduction

Tunable high selectivity bandstop filter design is one of the strategic Radio Frequency (RF) components in the front-end of civilian and military communication systems. This component has the potential to reduce the complexity and to relax the linearity requirements of the system by efficiently suppressing the unwanted signals before the LNA (Low-Noise Amplifier) of the RF front-end. It allows also to prevent the input of a wideband ADC (Analog to Digital Converter) from saturation and to optimize its dynamic range on weaker useful signals in the passband. This problem is actual in different system cases such as tactical military radio with a strong jammer, close transmitter and receiver positions, interferences (intentional or not) besides any established communication, heterogeneous levels in multi-standard wideband cognitive radio. Thus, low insertion loss in the passband zone, low-consumption power, compact size and high rejection with a constant depth over wide tuning range, are the expected objectives when it comes to design a tunable bandstop filter.

Despite the significant advances made in the area of tunable bandstop filter, less effort has been paid on designing bandstop filters with a constant rejection depth over the considered tuning range [4]-[11]. This issue may be intrinsically due to topology itself together with the frequency dependant behaviour of the low-cost substrate and/or the tuning elements (e.g. varactor diode, Pin diode, RF-MEMS). Moreover, as the coupling coefficient between the resonators and the main line is frequency dependant, the attenuation level changes proportionally. Thus, in order to be able to guarantee a constant rejection depth over the tuning range, these limitations have to be overcome. In [1], the authors propose a bandstop filter designed in UHF band and based on a traditional low-pass to bandstop frequency transformation. The circuit offers the possibility of having a constant depth over the considered band by using a tunable lumped inverter that controls, among other parameters, the rejection depth of the filter. In [2], a tunable active bandstop filter using a reconfigurable negative capacitance circuit is introduced to obtain a constant rejection depth by compensating for the passive element losses over the tuning range. This circuit offers a high constant rejection depth (-40 dB) but suffers from limited tuning range and linearity. In [3], a bandstop filter is implemented with two tunable resonators connected to each other by using a quarter-wavelength line. This filter topology features a constant bandwidth (related to the rejection depth) but requires choosing an optimum coupling coefficient, numerically calculated from the given equations. Moreover, the filter topology suffers from a large size and can be a bit complicated to set up.

Far from the traditional way to design a bandstop filter, a different approach based on channelized techniques can be used to generate bandstop filter response. Channelized filter techniques were mainly applied on designing band-pass filter applications [14]-[16] and very few research papers address the realization of bandstop filters [12]-[13]. In [12], the potential of channelized notch filter techniques was largely demonstrated. However, the frequency reconfiguration capability with a constant depth over the considered band and the high selectivity performances are obtained at the expense of: i) the number of circuit elements that increases the complexity and the circuit sensitivity and ii) the use of active components, such as amplifiers, that may compromise the system linearity and increase the power consumption. Very recently, a paper, that seems to follow an approach similar to the one described here, was proposed in [13]. The filter topology is a hybrid integration that combines Substrate Integrated Waveguide (SIW) resonator with a microstrip phase shifter. The circuit uses the same phase shifter [19] as the one used in this paper but for a different utility. Indeed, the phase shifter implemented in [13] is used as a bandwidth controller of the proposed bandstop filter. This use case differs from ours as the phase shifter in our paper was calculated and designed to have the higher rejection possible while keeping a constant rejection depth over the tuning range. Moreover, it's worth noting that our filter topology is fully designed using microstrip technology which have the advantage of having a

low cost, easy fabrication and reduced simulation cost over other technology such as SIW one.

This paper presents a tunable bandstop channelized filter composed of two branches, each of which contains a different function. The first branch integrates a tunable bandpass filter function while the other consists of a reconfigurable Phase-Shifter (PS). The topologies selected for both branches share two common characteristics, i.e. an implementation with coupled lines, and a rather identical frequency tuning range thanks to the same varactor diodes used in the two branches that offer the same capacitance values. Thereby, the combination of these two functions, with quite close topologies, allows achieving a tunable highly selective bandstop filter with a constant and high rejection level and a relatively wide tuning range in regards to the circuit simplicity. Synthesis equations are derived, used to describe the filter principle, and then applied to design a prototype. The corresponding simulated and measured results are compared and discussed to highlight the benefits of this proof-of-concept circuit.

2. Structure topology and analysis

In [17], it was demonstrated that a highly selective bandstop filter response can be obtained at a fixed frequency f_0 when a bandpass branch designed at f_0 is combined to a PS branch that acts as a bypass signal invertor network. In an ideal case, the output signal is cancelled at this frequency when the signals propagating through the two branches are combined at the output with the same amplitudes but with 180° of phase difference. In a real case, the attenuation level is degraded due to the difference that may exist between the amplitude and/or phase values of the combined signals. Far from the central frequency f_0, the bandpass filter acts as an open circuit and the signal at the input is simply driven to the output through the PS path to ensure the out of band response. As a result, the bandwidth of the global bandstop filter response is fully controlled by the the bandpass branch. In Figure 1, the global bandstop filter topology response is presented for different fractional bandwidth values of bandpass branch network having a central frequency at 700 MHz. It's shown from this figure that the global bandstop filter bandwidth varies as a function of the bandpass filter parameters.

Although the channelized two-branches bandstop filter works well for fixed frequency applications, the rejection depth of the bandstop filter becomes difficult to maintain when frequency tuning is needed. Thus, in order to extend the principle from a fixed-frequency version to a tunable one, the mutual cancellation conditions at the overall filter output must be adjusted and met for each desired frequency to be rejected. This means that both the PS and bandpass branches should be adjusted synchronously in order to maintain the rejection depth constant in the tuning range of the filter. Otherwise, the non-expected phase and magnitude differences between branches are likely to introduce impairments in the whole filter response.

The schematic block diagram of Fig.2 represents the tunable bandstop filter architecture. The analysis of this novel topology is done by first considering separately the two branches.

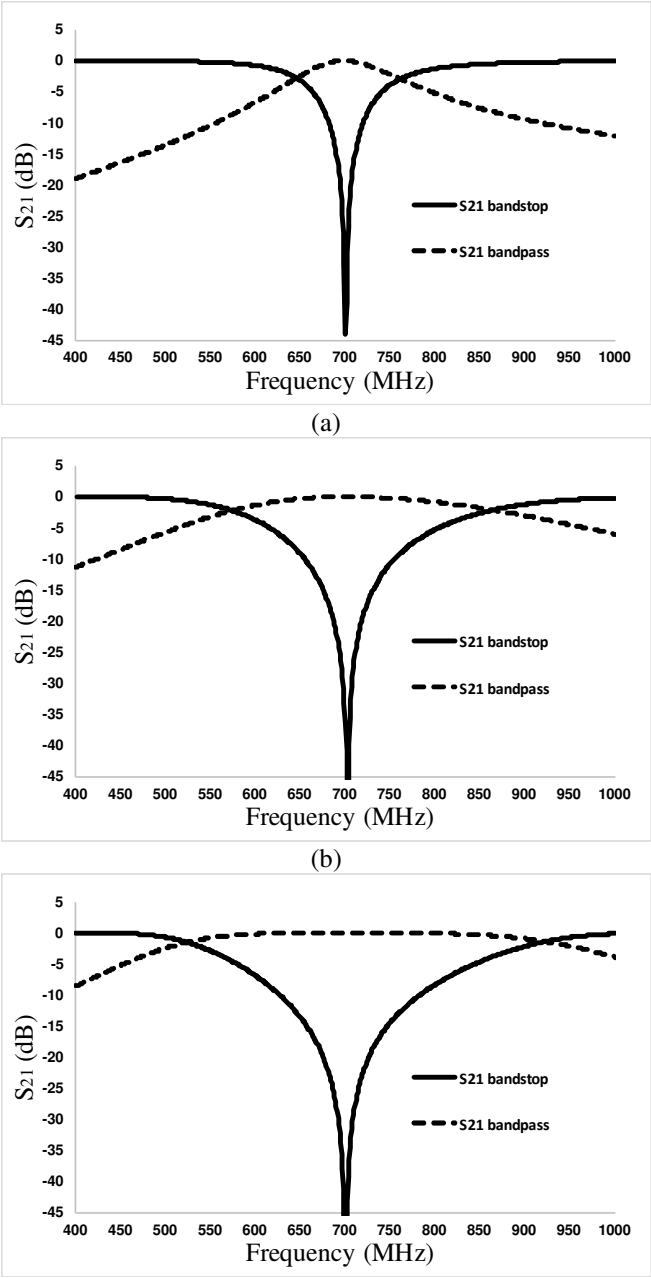

Fig. 1. *Evolution of the channelized bandstop bandwidth versus the bandwidth of the bandpass branch: (a) Fractional bandwidth of 17%. (b) Fractional bandwidth of 40% and (c) Fractional bandwidth of 70%.*

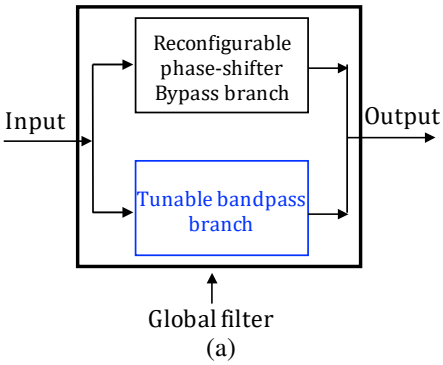

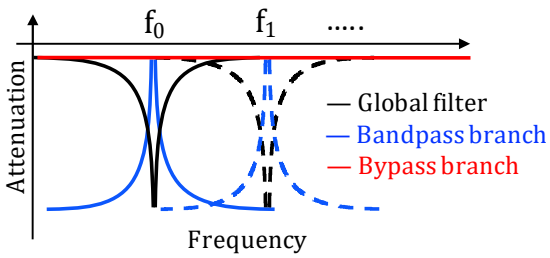

(b)

Fig. 2. *(a) Block diagram of the proposed tunable two-branches channelized passive bandstop filter. (b) Expected frequency tunable response.*

3. Tunable Bandpass Branch

The Bandpass filter topology considered here consists in parallel-coupled lines that use half-wavelength resonator. To introduce the frequency tunability in the bandpass branch response, two variable capacitors are loaded at the resonator ends as shown in Fig.3(a).

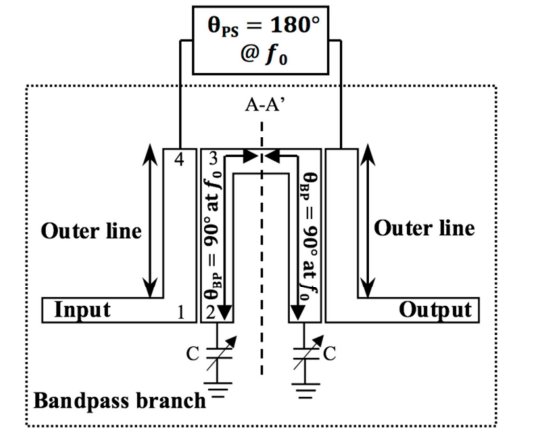

(a)

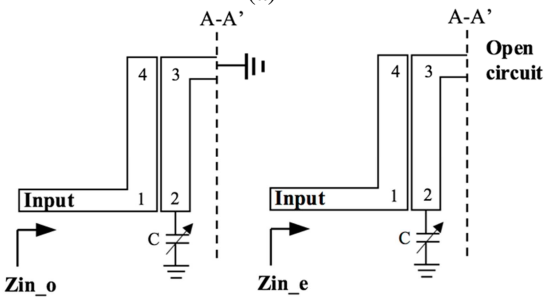

(b)

Fig. 3. *(a) 1st order tunable bandpass section. (b) Odd-mode and even-mode configurations of (a).*

From the A-A' symmetry plane, the even and odd modes equivalent circuits are extracted such as in Fig.3(b). By using the analysis method for coupled microstrip lines from [18], even- and odd-modes normalized input impedances (1)-(2) are extracted as a function of the impedance matrix.

$$Z_{in\_e} = \frac{Z_{11} - \left(\frac{Z_{12}^2}{Z_{cap} + Z_{11}}\right)}{Z_0} \tag{1}$$

$$Z_{in\_o} = \frac{Z_{11}^3 + Z_{11}^2 Z_{cap} - Z_{11}Z_{12}^2 - Z_{11}Z_{13}^2 - Z_{11}Z_{14}^2 + 2Z_{12}Z_{13}Z_{14} - Z_{13}^2 Z_{cap}}{Z_0(Z_{11}^2 + Z_{11}Z_{cap} - Z_{14}^2)} \tag{2}$$

where Z_{cap} is the equivalent impedance of the capacitor C, and Z_{ij} are the four-port matrix impedances of the coupled lines which port numbers are displayed in Fig.2(a).

The S-parameters of the bandpass branch network (Fig. 3) are written as:

$$S_{11} = S_{22} = \frac{Z_{in\_e} Z_{in\_o}}{(Z_{in\_e}+1)(Z_{in\_o}+1)} \tag{3}$$

$$S_{21} = S_{12} = \frac{Z_{in\_e} - Z_{in\_o}}{(Z_{in\_e}+1)(Z_{in\_o}+1)} \tag{4}$$

where z_{in_e} and z_{in_o} are the even- and odd mode normalized input impedances.

It comes from (3) that the bandpass network is matched at its input/output ports at $f=f_0$ ($S_{11}= S_{22}=0$) when:

$$Z_{in\_e} = \frac{1}{Z_{in\_o}} \tag{5}$$

This means that for the circuit to be reflection-less at the central frequency at f_0, the even and odd mode normalized input impedances at f_0 should be inversely proportional. Moreover, according to the resonance condition of $Z_{in\_o} = \infty$, equation (2) can be derived as:

$$Z_0(Z_{11}^2 + Z_{11}Z_{cap} - Z_{14}^2) = 0 \tag{6}$$

After straightforward manipulation of (6), the synthesis relation of the capacitor value C as a function of the expected resonant frequency f_0 of the bandpass filter is given by:

$$C = \frac{2\cot\theta}{(Z_{0e} + Z_{0o})\omega_0} \tag{7}$$

where C is the loaded capacitance value and θ, Z_{0e} and Z_{0o} are respectively the electrical length, the even and odd characteristic impedances of the coupled line and ω_0 the angular frequency.

Thus, by introducing in (4) inversely proportional even- and odd-mode impedances at $f=f_0$ leads to S_{21} equal to -1, meaning that the input signal power is transmitted to the outport port of the band-pass branch with a -180° change in phase.

For demonstration purpose, the synthesized capacitor values C obtained from (7) are plotted as a function of the resonant frequency and shown in Fig. 4, using the following parameters: Z_{0e} = 75 Ohm, Z_{0o} = 38 Ohm, θ=90° at f_0 = 700 MHz. Following that synthesis method, an ideal first order coupled line bandpass branch network with a fractional bandwidth FBW=0.17 at f_0 = 700 MHz was simulated using Advanced Design System software. As it can be noticed in Fig. 5(a), the bandpass filter resonates at the expected resonance frequencies as a function of the loaded capacitor values extracted from (7). It should be pointed out that only single bias voltage is needed for both varactors of the bandpass filter branch.

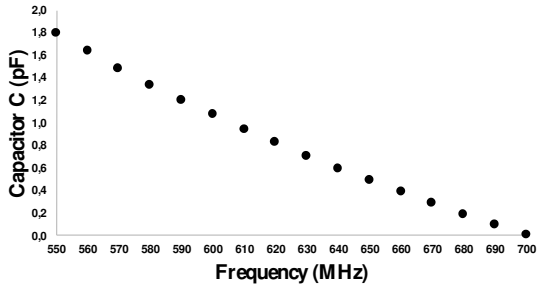

Fig. 4. Synthesized capacitor values of the bandpass branch as a function of the needed resonant frequency.

As expected, (see Fig.5(b)), the portion of the signal traveling through the bandpass branch at the central frequencies f_0 is shifted by -180°. On the other hand, as the coupled-line section acts as a 3dB-coupler with an equal split, the other portion of the signal is also shifted naturally by approximatively -180° since it passes through the two outer lines (-90° for each coupled-line section, see Fig. 3(a)). Then, to allow the two signals to combine in opposite signs at the global filter output, the PS itself should shift the signal also by -180°. Moreover, the PS branch should also be tunable to follow synchronously the change of the bandpass central frequency and to allow the two signals to combine in a destructive manner at the global filter output.

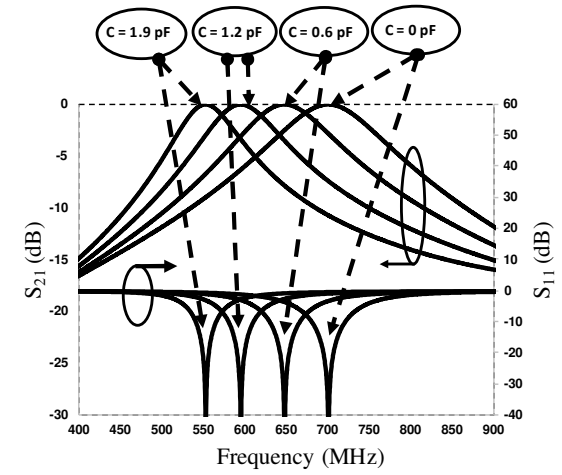

(a)

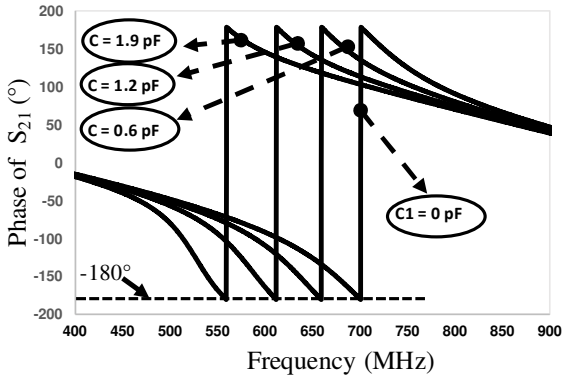

(b)

Fig. 5. S-parameters (a) and transmission phase (b) response of the bandpass network branch as a function of the capacitor values extracted from (7).

4. Reconfigurable Phase Shifter Bypass Branch

The reconfigurable PS bypass branch considered in this paper [19] is presented in Fig.6. Besides its advantages in terms of compactness and easy implementation, this all-pass PS topology affords an interesting compromise between phase variation range versus the varactor tuning range, insertion and return losses, while using a single voltage control.

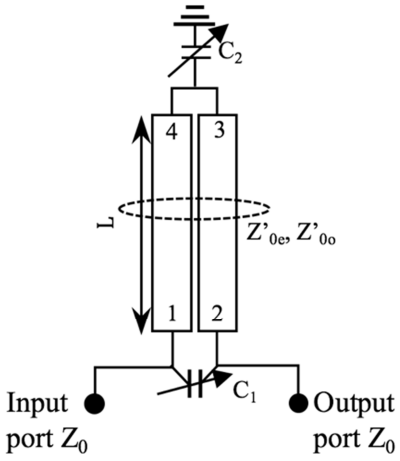

Fig. 6. Topology of the reconfigurable Phase Shifter used in the bypass branch.

According to Fig. 6, by using the even and odd analysis, the transmission phase of the reconfigurable PS can be expressed as follows:

$$\psi_{21} = -\frac{\pi}{2} + \tan^{-1}\left(\frac{1}{2Z'_{0e}Z'_{0o} - \tan\theta C_2 \omega Z'^{2}_{0e} Z'_{0o}} \left(Z_0 \left(\begin{array}{c} -Z'_{0o}\tan\theta + Z'_{0e}\cot\theta + \\ \tan\theta C_1 C_2 \omega^2 Z'^{2}_{0e} Z'_{0o} - \\ 2C_1 \omega Z'_{0e} Z'_{0o} - \\ \frac{C_2}{2}\omega Z'_{0e} Z'_{0o} \end{array} \right) \right) \right) \quad (8)$$

where Z_{0e}' and Z_{0o}' are respectively the even and odd characteristic impedances of the PS coupled line, $Z_0 = 50\ \Omega$ is the port reference impedance , θ is the electrical length of the coupled line, and C_1, C_2 are the variable capacitors.

As a first approximation [19], the input impedance of the reconfigurable PS yields to a matched input condition when:

$$C_2 = 2C_1 \text{ and } Z'_{0e} = \sqrt{2} Z_0 \quad (9)$$

According to (8), the transmission phase Ψ_{21} is of -180°, when the component inside the $\tan^{-1}$ function is set to $-\infty$. Therefore, the following relation can be expressed as:

$$2Z'_{0e}Z'_{0o} - \tan\theta C_2 \omega Z'^{2}_{0e} Z'_{0o} = 0 \quad (10)$$

By substituting the conditions from (9) into (10), the capacitor value C_1 that allows getting -180° of phase shift at a specific frequency f_0 is given by:

$$C_1 = \frac{1}{2\pi f_0 Z'_{0e} \tan\theta} \quad (11)$$

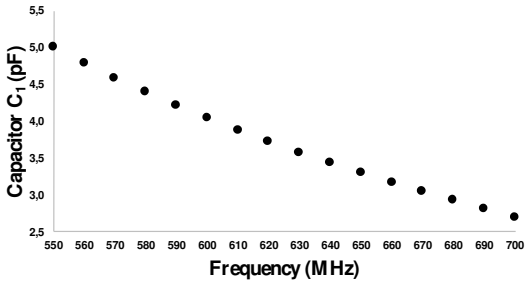

Fig. 7. *Loaded capacitance values of the reconfigurable PS network corresponding to -180° versus frequency.*

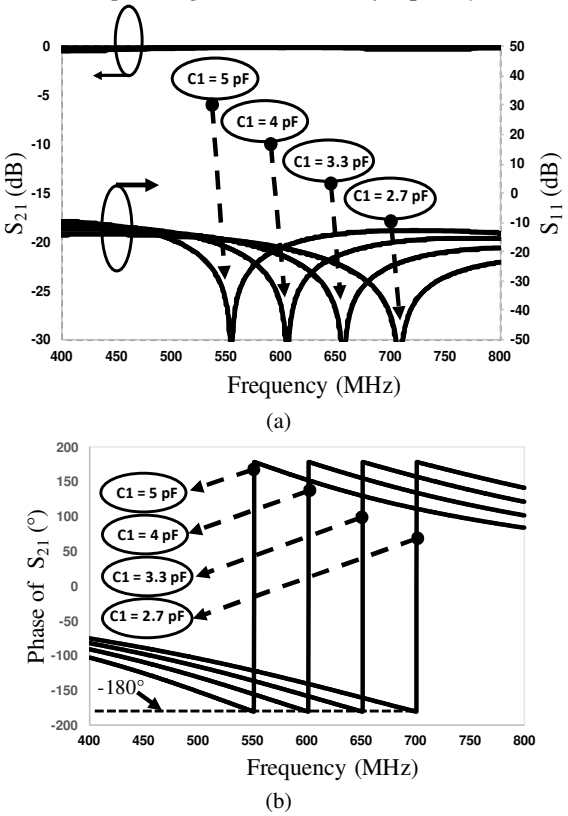

Fig. 8. *S-parameters (a) and transmission phase (b) response of the reconfigurable PS network branch as a function of the loaded capacitance value.*

To verify the validity of equation (11), the capacitor values C_1 (pF) curve derived from this equation is plotted as a function of the frequency at which the phase inversion occurs (S_{21} phase = -180°). Fig. 7 shows the calculations of the extracted capacitor values with the following parameters: Z_{0e} = 70.7 Ohm (in regards to equation (9)) θ=90° at 1.8f_0 (1260 MHz) as a trade-off between small physical size and needed capacitor values. The ideal all-pass PS simulations confirm a good input and output matching in the entire considered band for all capacitor values (Fig. 8(a)), as well as the required phase inversion over the expected frequency-tuning range (Fig. 8(b)). It should also be pointed out that only single bias voltage is needed to control the varactor diodes used in the PS branch.

5. Two Branches Tunable Bandstop Filter

To demonstrate the proposed approach, the two tunable branches described above are connected to each other as shown in Fig. 9 (a). The bandpass resonator branch is designed to be half-wavelength at the maximum frequency of the considered range (at f_0=700 MHz). This resonator was loaded, at each extremity, by varactor diodes (Fig. 3 (a)) to ensure its agility from 550 – 700 MHz. On the other hand, the bypass PS branch is designed to be quarter-wavelength at 1.8 f_0 as discussed in the previous section. Indeed, designing this coupled-line all-pass PS to be quarter-wavelength at higher frequencies bring directly a compactness improvement, together with the possibility to operate over wide band while offering an interesting $\Delta\varphi/\Delta C_1$ ratio. In order to allow the PS branch to be adjusted, three varactor diodes are loaded and controlled by a single voltage control.

The global filter structure was fully simulated using Momentum tool of Agilent ADS software on low-cost 1.56-mm-thick FR4 substrate (h = 1.56 mm, ε_r = 4.3, tan δ= 0.02). The Infineon BB837 silicon varactor diode (0.5 – 6 pF) is used for C, C_1 and two in parallel for C_2 (C_2 =2C_1). Fig. 9 (c) shows the photograph of the fabricated two-branches channelized passive filter on FR4 substrate. The measured results of the global filter are shown in Fig. 9 (b) and a good agreement is noticed compared to the simulation results. The proposed filter provides a tunable constant bandstop response with a constant and relatively high rejection depth (20 dB). The varactor diodes of C and C_1 are tuned from 0.5 to 2 pF and from 2.8 to 5 pF, respectively, to allow the central frequency to be tuned from 550 to 700 MHz. Moreover, the circuit presents low insertion loss (0.6 dB) in the pass-band areas of the filter while the input/output ports always stay matched. The response stability versus the tuning bias has to be highlighted. Indeed, the rejection level and bandwidths, the matching level and the insertion loss remains rather constant along the frequency range. The use of coupled-line sections and identical varactors in each branch create a common response behaviour versus tuning bias, which, a priori, contribute to a decrease of the whole response discrepancies.

The work presented in this paper has been compared to some works already published in the literature. The comparison is summarized in table 1. As it can be noticed from this table, the proposed circuit is a good compromise when it comes to design a tunable stop-band filter that takes into account many parameters at the same time, such as: a constant rejection depth, compact size, low consumption power, etc.

Table 1 Comparison with some previous work

Ref.	Used technology	Resonator type	Order	Range (GHz)	Tuning percent (%)	Passband insertion Losses (dB)	$\Delta\alpha$* (dB)
[2]	Microstrip	Active	1	0.75 – 0.85	12%	0.6 dB at 50 MHz far from f_0	Constant rejection depth
[5]	Microstrip	Passive	2	0.53 – 1.48	94%	-	14
[6]	multi-layer PCB	Passive	2	2.15 – 2.75	24%	2.5 dB at 300 MHz far from f_0	8
[7]	Silicon	Passive	1	3.5 – 6.5	60%	<1 dB at 8 GHz far from f_0	22
[9]	Microstrip	Passive	2	0.58 – 1.07	59%	0.58 dB	15
[12]	hybrid-integrated	Active	-	9.5 – 10.5	10%	1.6 dB at 6 GHz far from f_0	constant rejection depth
[13]	Hybrid - SIW	Passive	1	2.8 – 3.4	19%	-	13
[This work]	Microstrip	Passive	1	0.55 – 0.75	30%	0.6 dB at 200 MHz far from f_0	constant rejection depth

Where $\Delta\alpha$ is the difference in rejection depth (dB) between the upper and lower central frequency of the proposed filter. Indeed, the higher the value of $\Delta\alpha$, the bigger the difference in rejection depth between upper and lower central frequency.

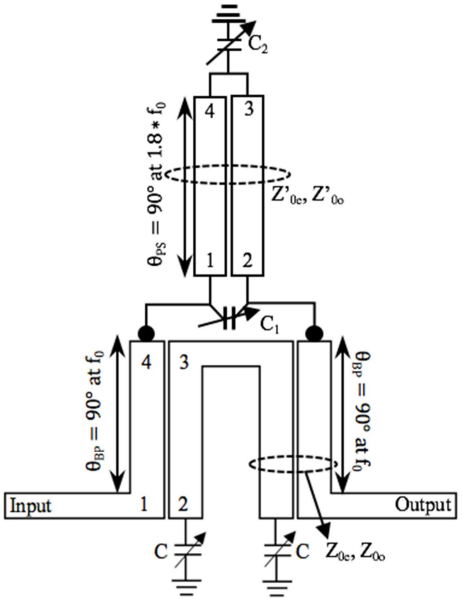

(a)

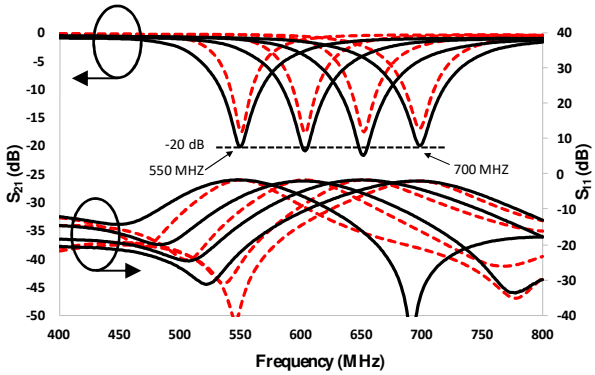

(b)

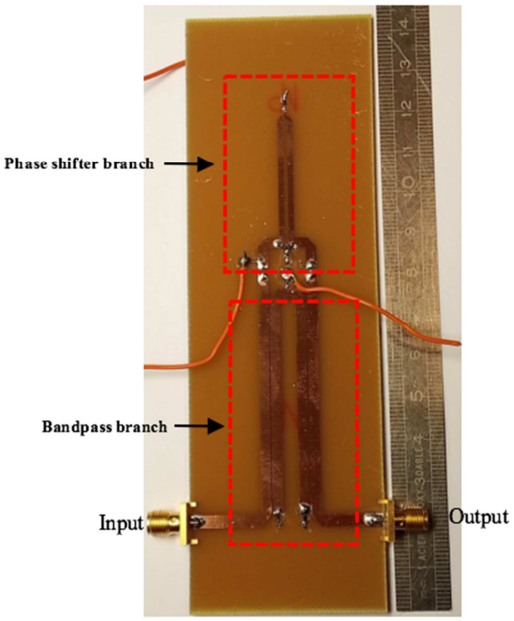

(c)

Fig. 9. (a) Schematic, (b) Simulated (dashed lines) and measured (solid lines) S-parameters and (c) photograph of the tunable two-branches passive bandstop filter.References

6. Conclusion

A tunable bandstop channelized passive filter is designed with satisfactory insertion loss, good input/output match, and a relatively wide tuning range. The derived analytical design formulas of the different varactor diode values that allow the filter to have the optimum performance at the needed frequency are provided. The availability of synthesis relations together with an easy to implement and

to control topology make this tunable channelized filter suitable for various technology implementation (hybrid, integrated CMOS, MMIC, …) for Software Defined Radio, Cognitive Radio systems or any system that requires a frequency-agile bandstop filter. In the case of applications that require a higher attenuation level, it's possible to form a higher order filter by cascading this first order filter topology to achieve the requested rejection level. As a result, only two bias voltages are needed to tune the cascaded bandstop filter (one for the bandpass branches and another one for the PS branches). Thus, the frequency tunability behavior of the cascaded higher order bandstop filter is highly simplified.

7. References

[1] Y.-C. Ou and G. M. Rebeiz, "Lumped-Element Fully Tunable Bandstop Filters for Cognitive Radio Applications," IEEE Transactions on Microwave Theory and Technique., vol. 59, issue: 10, pp. 2461 – 2468, Oct. 2011.

[2] R. Lababidi, J. Lintignat, B. Jarry, B. Barelaud, A. Louzir, D. Lo Hine Tong, "Highly compact tunable stop-band active filter for advanced communication systems," Analog Integrated Circuits and Signal Processing., vol. 77, issue: 2, pp. 207–219, Nov. 2013.

[3] X. Y. Zhang, C. H. Chan, Q. Xue, and B. J. Hu, "RF tunable bandstop filters with constant bandwidth based on a doublet configuration," IEEE Trans. Ind. Electron., vol. 59, no. 2, pp. 1257–1265, Feb. 2012.

[4] T. Ching-Wen, C. Wei-Chen, "A Compact Tunable Notch Filter With Wide Constant Absolute Bandwidth," IEEE Microwave and Wireless Components Letters., Vol. 25, issue: 3, pp. 151– 153, March 2015.

[5] H. Xiao, "A Novel Planar Tunable Bandstop Filter Based on Simple Coupled-line," IEEE International Conference on Network Infrastructure and Digital Content. September 2012.

[6] T. Yang and G. M. Rebeiz, "Bandpass-to-bandstop reconfigurable tunable filters with frequency and bandwidth controls," IEEE Trans. Microw. Theory Techn., vol. 65, no. 7, pp. 2288–2297, Jul. 2017.

[7] Z. Wu, Y. Shim and M. Rais-Zadeh, "Miniaturized UWB Filters Integrated with Tunable Notch Filters Using a Silicon-Based Integrated Passive Device Technology," IEEE Transactions on Microwave Theory and Techniques vol. 60, Issue. 3, Marc. 2012.

[8] M. F. Karim, A. Q. Liu, A. B. Yu, and A. Alphones, "MEMS-based tunable bandstop filter using electromagnetic bandgap (EBG) structures," in Proc. Asia–Pacific Conf. Microw. Conf. (APMC), vol. 3. Dec. 2005, p. 4.

[9] J. Cai, Y-J. Wang, W. Qin and J-X Chen, "Wideband Tunable Differential Bandstop Filter Based on Double-Sided Parallel-Strip Line," IEEE Transactions on Components, Packaging and Manufacturing Technology. February 2018.

[10] I. Reines, S-J. Park, G. Rebeiz, "Compact Low-Loss Tunable -Band Bandstop Filter With Miniature RF-MEMS Switches", IEEE Transactions on Microwave Theory and Techniques, Vol. 58, No.7, July 2010.

[11] I. Gil, J. Garcia-Garcia, J. Bonache, F. Martin, M. Sorolla and R. Marques, "Varactor-loaded split ring resonators for tunable notch filters at microwave frequencies", ELECTRONICS LETTERS 14th October 2004 Vol. 40 No. 21.

[12] C. Rauscher, "Varactor-tuned active notch filter with low passband noise and signal distortion," IEEE Transactions on Microwave Theory and Techniques., vol. 49, issue: 8, pp. 1431 – 1437, Aug. 2001.

[13] S-W Jeaong and J. Lee, "Frequency- and Bandwidth-Tunable Bandstop Filter Containing Variable Coupling Between Transmission Line and Resonator" IEEE Transactions on Microwave Theory and Techniques, Vol. 66, NO. 2, February 2018.

[14] R. Gomez-Garcia, J. I. Alonso, C. Briso-Rodriguez, "On the design of high-linear and low-noise two-branch channelized active bandpass filters," IEEE Transactions on Circuits and Systems II: Analog and Digital Signal Processing., vol. 50, issue: 10, pp. 695 – 704, Oct. 2003

[15] C. Rauscher, "Two-Branch Microwave Channelized Active Bandpass Filters," IEEE Transactions on Microwave Theory and Techniques., vol. 48, issue: 3, pp. 437 – 444, Mar. 2000.

[16] S. Darfeuille, J. Lintignat, R. Gomez-Garcia, Z. Sassi, B. Barelaud, L. Billonet and B. Jarry, "Silicon-Integrated Differential Bandpass Filters Based on Recursive and Channelized Principles and Methodology to Compute Their Exact Noise Figure", IEEE Transactions on Microwave Theory and Techniques, Vol. 54, NO.12, December 2006.

[17] R. Lababidi, M. Le Roy, D. Le Jeune, A. Perennec, R. Vauche, S. Bourdel, J. Gaubert, "Compact highly selective passive notch filter for 3.1–5 GHz UWB receiver system," 2015 IEEE International Conference on Electronics, Circuits, and Systems., 6-9 Dec. 2015.

[18] R.J. Wenzel, "Exact Design of TEM Microwave Networks Using Quarter-Wave Lines," IEEE Transactions on Microwave Theory and Techniques., vol. 12, issue: 1, pp. 94-111, Jan. 1964.

[19] K. Khoder, A. Pérennec, and M. Le Roy, "A 180° tunable analog phase shifter based on a single all-pass unit cell," Microw. Opt. Technol. Lett., vol. 55, no. 12, pp. 2915–2918, 2013.